Available online at www.sciencedirect.com
SCIENCE DIRECT®
Biomaterials 24 (2003) 4181–4190
Biomaterials
www.elsevier.com/locate/biomaterials

Structure and mechanical properties of poly(D,L-lactic acid)/poly(ε-caprolactone) blends ☆

M.E. Broz[1], D.L. VanderHart, N.R. Washburn*

Polymers Division, National Institute of Standards and Technology, Gaithersburg, MD 20899, USA

Received 13 November 2002; accepted 8 April 2003

Abstract

A series of blends of the biodegradable polymers poly(D,L-lactic acid) and poly(ε-caprolactone) were prepared by varying mass fraction across the range of compositions. Tensile testing was performed at room temperature using an extensometer and the elastic modulus was calculated for each blend. The blends were also tested to failure, and the strain-at-failure and yield stress recorded. While the blend has been shown to have a lower critical solution temperature, the mechanical properties were insensitive to the annealing conditions. Scanning electron microscopy was used to characterize the blend microstructure and poor adhesion was observed at the interface between blend components. Differential scanning calorimetry was performed but the results were somewhat variable, indicating this blend may have complex phase behavior that depends sensitively on the method of preparation. However, nuclear magnetic resonance data indicate the two components are phase separated. A percolation model is used to explain the observed mechanical data and the results are consistent with the predictions of the Kerner–Uemura–Takayangi model. The results of these experiments demonstrate the utility of polymer blending in tuning material properties.
Published by Elsevier Science Ltd.

Keywords: Mechanical properties; Microstructure; Polycaprolactone; Polylactic acid

1. Introduction

Many medical technologies involve the use of synthetic materials, ranging from common products such as sutures to developing products such as scaffolds for tissue engineering. Numerous biodegradable polymers are approved for use, some of the most common being polyesters such as poly(lactic acid) (PLA), poly(glycolic acid) (PGA) and poly(ε-caprolactone) (PCL). These aliphatic polymers degrade by hydrolytic or enzymatic pathways, making them suitable for medical uses. PLA and PGA have glass transition temperatures above room temperature, rendering them hard and brittle. However, PCL is crystalline and has a low glass transition temperature so is tough but has a modulus an order of magnitude smaller than PLA [1]. However, these properties are not ideal for all applications. In order for polymers to be useful, it is necessary to be able to tune the material properties to satisfy engineering constraints. The mechanical response of polymers is characterized as a competition between elastic and plastic deformation [2] and one well-established strategy for tuning material properties is to blend two polymers [3].

Blending can radically alter the resultant properties, which depend sensitively on the mechanical properties of the components as well as the blend microstructure and the interface between the phases. The polymers may be amorphous or semi-crystalline, glassy or elastomeric, and miscible or immiscible, and the structure and properties of the resultant blend will be strongly influenced by the processing conditions [4]. In blends of immiscible, amorphous polymers A and B with low mass fraction of polymer A, this component tends to form isolated droplets in a continuous matrix of polymer B. At higher mass fractions of polymer A, the

☆ Certain equipment and instruments or materials are identified in the paper in order to adequately specify the experimental details. Such identification does not imply recommendation by the National Institute of Standards and Technology, nor does it imply the materials are necessarily the best available for the purpose. According to ISO 31-8, the term "molecular weight" has been replaced by "relative molecular mass," M_r. The conventional notation, rather than the ISO notation, has been used for this article.

*Corresponding author. Fax: +1-301-975-4977.
E-mail address: newell.washburn@nist.gov (N.R. Washburn).
[1] Current address: Department of Chemical Engineering and Materials Science, University of Minnesota, Minneapolis, MN 55455, USA.

0142-9612/03/$ - see front matter Published by Elsevier Science Ltd.
doi:10.1016/S0142-9612(03)00314-4

droplets coalesce and the blend forms a co-continuous structure; this process can be described by percolation theory. At even higher mass fractions of polymer A, polymer B forms droplets in a matrix of A. The composition of the percolation threshold is a function of the blend interfacial tension as well as the viscoelastic properties of the polymers [5,6]. Crystallization of one or both components complicates this relatively simple picture.

Several semi-crystalline/glassy polymer blends have been investigated, including poly(aryl ether ether ketone)/poly(ether imide) (PEEK/PEI) [7] and high-density polyethylene/polycarbonate (HDPE/PC) [8–10]. PEEK/PEI is an example of a miscible blend while HDPE/PC is immiscible. Using differential scanning calorimetry (DSC), Harris and Robeson characterized the degree of blending in PEEK/PEI blends [7]. The PEEK samples used in their investigation had glass transition temperatures of 142°C and 152°C and melting temperatures of 337°C and 361°C, respectively, while the PEI had a glass transition temperature of 215°C but did not crystallize. After crystallizing blends at 300°C, the authors measured melting temperatures that were essentially unchanged from those measured in the pure PEEK samples and a single, sharp glass transition temperature in all samples that obeyed the Fox equation

$$\frac{1}{T_g} = \frac{w_1}{T_{g1}} + \frac{w_2}{T_{g2}}, \quad (1)$$

where w_A is the mass fraction of polymer A and T_{gA} the glass transition temperature. This indicates that PEI is excluded from PEEK crystallites, thus leaving T_m unchanged, but forms a single phase in the amorphous regions of the blend, which leads to systematic variations in T_g.

The importance of interfacial adhesion was stressed by LeClair and Favis [10], who observed rather surprising interfacial behavior in the HDPE/PC blend. At compositions where the continuous phase was comprised of semi-crystalline HDPE, good interfacial adhesion was observed with the PC droplets. However, when the continuous phase was amorphous PC, the interface with the HDPE droplets was sharp, suggesting a complete absence of adhesion. The models of Kerner [11] and Uemura and Takayanagi [12] can be used to fit the observed mechanical properties for the droplet blend morphology in the extreme cases of perfect adhesion or no adhesion.

In this work, we investigated the structural and mechanical properties of PLA/PCL blends. Both polymers have been widely used in a variety of medical applications and, to our knowledge, there has not been a systematic investigation of the mechanical properties of these blends. This system was of particular interest because the components were shown to have a lower critical solution temperature (LCST) at a PCL volume fraction of 36% and a temperature of 86°C [13]. The phase diagram is reproduced in Fig. 1 and displays the inverted, asymmetric shape usually associated with LCST blends. The melting point of PCL is 65°C and is marked by a dashed line in the figure. Above this temperature but below the LCST, the blend is miscible across the composition range. However, annealing the blend in the two-phase region will induce phase separation, with compositions of the two phases set by the positions of the phase boundary and volume fractions fixed by the lever rule. We hypothesized that blends annealed in the single-phase region would have enhanced interfacial adhesion between crystalline and non-crystalline domains as compared to blends annealed in the two-phase region, leading to significant changes in mechanical properties.

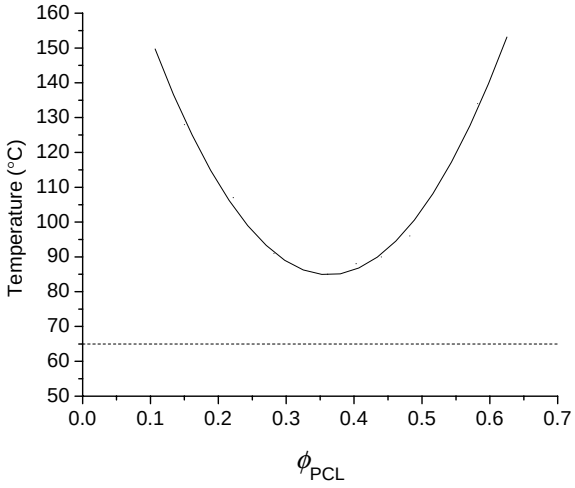

Fig. 1. The temperature–composition phase diagram for the PLA/PCL blend (adapted from [13]) with the LCST at PCL mass fraction 0.36°C and 86°C. The solid curve represents the phase boundary and the inverted, asymmetric shape is characteristic of LCST-type behavior. The dashed line represents the melting point of PCL and above this temperature but below the phase boundary, the blend components are miscible.

We report here the strain-at-failure, yield stress, and Young's modulus of PLA/PCL blends over the full mass fraction range. Scanning electron microscopy was used to characterize blend microstructure. DSC and nuclear magnetic resonance (NMR) experiments were also performed in order to better understand the results of the mechanical tests.

2. Experimental

2.1. Materials

The PLA was obtained from Polysciences with $M_W = 100,000$ and the PCL was obtained from Aldrich with

$M_W = 80,000$. Both polymers were used as received. PLA and PCL blends were prepared by dissolution in methylene chloride (Fisher) with a total polymer mass fraction of 10%. The solutions were cast onto Kapton® or Teflon® surfaces as a thin film. Residual solvent was removed by vacuum drying at 80°C for at least 24 h. The blends were removed from the film and stored in Petri dishes sealed with Parafilm at 4°C. A 25/75 blend was also mixed for 5 min in a mini-compounder (Daca Instruments, Goleta, CA) at 100°C and 157 rad/s (50 rpm).

2.2. Mechanical testing

Blends were pressed at 80°C or 150°C for 60 min to remove bubbles and to allow equilibration in the one- or two-phase regions of the phase diagram. They were then melted into a 1 mm × 4 mm silicone dog bone mold, and pressed in the hot press at 80°C or 150°C. The samples were allowed to cool at room temperature under atmospheric pressure. Tensile testing was performed at room temperature on an Instron 5500R, at cross-head speeds of 1 and 0.1 mm/min with a 5 kN load cell. No rate dependence for the modulus was observed during mechanical testing suggesting viscoelastic effects were not important at these strain rates. A 10-mm extensometer was used to collect low-strain data to measure the Young's modulus. Samples were also pulled to higher strains to record the strain-at-failure and yield stress, which is the term used here to describe both yield stress of plastic materials and ultimate tensile strength of glassy materials. Measurements were made on pure blend components that were solvent cast and those that were pressed without the use of solvent to validate the conditions used for blend preparation. No significant difference was observed, suggesting that these annealing conditions were sufficient to remove residual solvent. The error bars in the figures represent one standard deviation and are taken as the standard uncertainty.

2.3. Differential scanning calorimetry

The thermal properties of the blends were analyzed using a Perkin-Elmer DSC 7. Samples were tested by heating from 0°C to 100°C, at a rate of 10°C/min under helium. Melting and glass transition temperatures (T_m and T_g, respectively) were recorded by monitoring the peaks of the endotherms.

2.4. Scanning electron microscopy

Samples were fractured in liquid nitrogen and sputtered with gold prior to imaging. Electron micrographs were obtained with a JEOL-JL-5300 operating at 15 kV and 50 mA.

2.5. Nuclear magnetic resonance

300 MHz proton NMR spectra were obtained on PLA–PCL blends at ambient temperature (21°C) using a Bruker Avance spectrometer (Bruker Biospin, Billerica, MA). Measurements were performed using a low-background proton probe (Doty Scientific, Inc., Columbia, SC). The magic angle spinning (MAS) rate was 2525 Hz. Radiofrequency field strength corresponded to a 167 kHz proton nutation frequency (1.5 μs 90° pulse). Spectrometer dead time was 2 μs for the Bloch-decay spectra.

3. Results and discussion

3.1. Mechanical properties

A characteristic run from the tensile testing of a 60% PLA sample is shown in Fig. 2. After an initial regime where the sample relaxes into the grips, the linear strain regime is observed at strains below 0.04 and the slope is used to calculate the modulus using the cross-section of the testing bar. The yield point is observed at a strain of 0.042, which is used as a measure of the material brittleness. The stress at which this occurs is taken as the yield stress even though this quantity is somewhat ill-defined for brittle materials. Necking occurs after yielding and may extend to high strains, depending on the toughness of the blend.

Shown in Fig. 3 are the strain-at-failure data across the entire mass fraction range. This value decreases

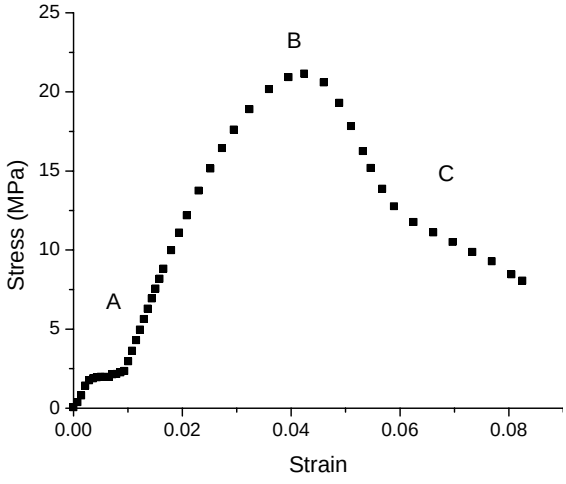

Fig. 2. A representative tensile test plot of applied force as a function of displacement for the 40/60 blend. The modulus is taken as the slope of the linear part of the curve (region A) divided by the pre-test sample cross-section. Point B denotes the yield or failure point (used synonymously to describe the strain at which the peak stress is recorded) of the sample and region C is where necking is observed. The estimated uncertainty of these measurements is 5%.

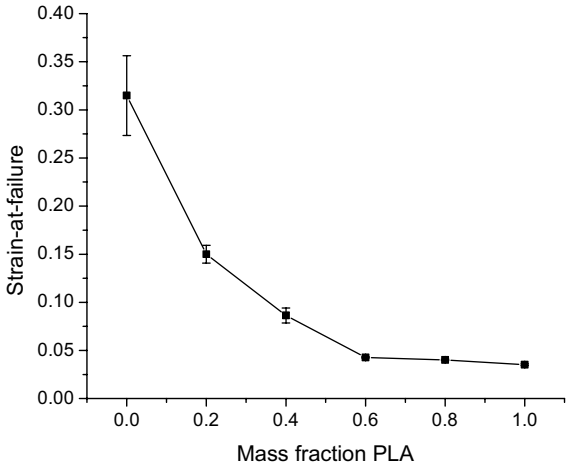

Fig. 3. Plot of strain-at-failure across the composition range for the PLA/PCL blends. The monotonic decrease below PLA mass fraction 0.5 is consistent with diluting the PCL matrix with PLA inclusions. The near-constant value above PLA mass fraction 0.5 is consistent with the glassy PLA phase forming a brittle matrix. The standard uncertainty is denoted by the error bars, which represent the standard deviation over multiple measurements.

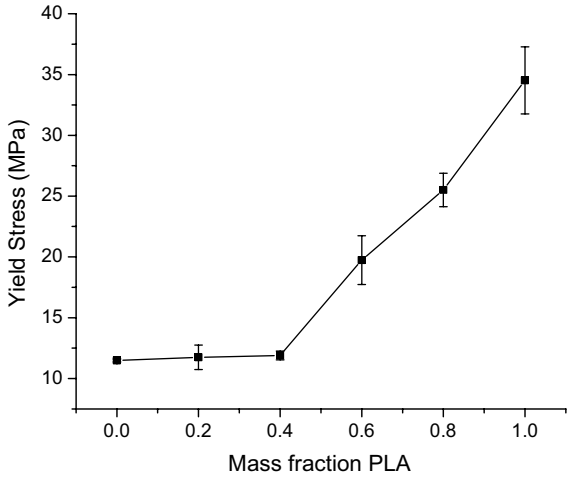

Fig. 4. Plot of yield stress as a function of blend composition. The flat behavior at low PLA content suggests there may be some toughening to compensate for the decrease in PCL matrix volume. Above the PLA mass fraction of 0.5, the monotonic increase in ultimate tensile strength suggests there is little toughening due to blending in this regime. The standard uncertainty is denoted by the error bars, which represent the standard deviation over multiple measurements.

monotonically as the mass fraction of PLA increases. A rather precipitous drop is seen from 0 to 0.6 followed by flat behavior thereafter. This indicates that even small amounts of glassy PLA are capable of embrittling the PCL matrix; at PLA mass fraction 0.2 the strain-at-failure has decreased 50% relative to pure PCL. This may be due to blending of the glassy PLA into the PCL matrix or simply to the formation of PLA inclusions in the blend with some interfacial adhesion, and the results on structural investigations using SEM and NMR give some insight into this. The flat part of the curve at PLA mass fractions at and above 0.6 is consistent with the formation of a continuous PLA matrix; PLA is glassy and the strain-at-failure is expected to be insensitive to strain because it depends on molecular parameters such as the free volume in the matrix phase [14]. If this hypothesis were true, it suggests that there is very little mixing between PLA and PCL in this composition range; otherwise, the PCL would have been expected to have a toughening effect on the blend. Therefore, it appears that there may be some association of PLA and PCL at low PLA mass fraction but at higher PLA contents there is little or no reinforcement due to blending.

In Fig. 4, the yield stress data as a function of composition are shown. The yield stress is insensitive to composition from PLA mass fraction 0–0.4 then increases linearly up to 1.0. This linear dependence of yield stress at compositions ranging from pure PLA down to PLA mass fraction 0.6 suggests PCL blending in this regime simply dilutes the PLA matrix like the presence of voids in the material, reducing the total stress necessary to fracture the samples. The flat trend at compositions ranging from pure PCL to PLA mass fraction 0.4 suggests there must be some reinforcement due to interactions between PLA and PCL, otherwise a similar reduction in yield stress in blended samples would be observed as in the PLA-rich samples.

In Fig. 5, a plot of Young's modulus as a function of blend composition is shown, represented as the solid line. The modulus is relatively flat for mass fractions of PLA at and below 0.4 then increases linearly as the fraction of PLA increases. The trends in the Young's modulus were fit using the Kerner–Uemura–Takayanagi model [11,12], which treats the blend as spherical inclusions of polymer 2 having Young's modulus E_2 in a continuous matrix of polymer 1 having Young's modulus E_1 and Poisson's ratio v_1, taken to be 0.5. It was assumed that at PLA mass fractions less than 0.5, PCL formed the continuous matrix and above 0.5, PLA formed the continuous matrix. Two variations in this model assume either perfect adhesion at the blend interface or complete absence of adhesion. The form of the equation that assumes zero interfacial adhesion between blend components (shown as the dashed line in Fig. 5) is

$$E = E_1 \frac{(7-5v_1)E_1 - (7-5v_1)E_1\phi_2}{(7-5v_1)E_1 + (8-10v_1)E_1\phi_2} \quad (2)$$

given a better fit at higher PLA mass fraction. The fit is quite good at PLA mass fractions above 0.5 but the theory underestimates the blend modulus at lower PLA mass fractions. This may indicate the existence of interfacial bonding and the modified version of the this equation that assumes perfect adhesion was used to predict the modulus using Eq. (3) (shown as the dotted

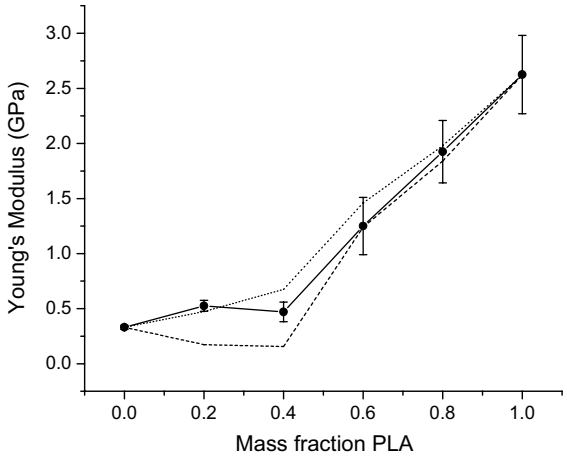

Fig. 5. Plot of Young's modulus as a function of blend composition (solid line). The modulus increases monotonically as a function of increasing PLA content. Also shown are fits to the Kerner–Uemura–Takayanagi theory assuming the phase with mass fraction greater than 0.5 constitutes the matrix. The dashed line represents the fit assuming zero interfacial adhesion and the dotted line represents the fit assuming perfect adhesion. The modulus at PLA mass fractions below 0.5 suggests there may be some toughening at the PLA–PCL interface. The standard uncertainty is denoted by the error bars, which represents the standard deviation over multiple measurements.

line in Fig. 5)

$$E = E_1 \frac{(7-5\upsilon_1)E_1 + (8-10\upsilon_1)E_2 - (7-5\upsilon_1)(E_1-E_2)\phi_2}{(7-5\upsilon_1)E_1 + (8-10\upsilon_1)E_2 + (8-10\upsilon_1)(E_1-E_2)\phi_2}. \quad (3)$$

Eq. (3) appears to offer a better prediction of the modulus at PLA mass fractions of 0.2 and 0.4, suggesting that some association between PLA and PCL exists at these compositions.

On the basis of the mechanical testing data, it appears that some reinforcement occurs when a PLA-rich blend is prepared but in PCL-rich blends, the blend behavior suggests there is no physical association between the blend components. It is interesting to note that this is qualitatively similar to the behavior observed by LeClair and Favis [10] in their study of HDPE/PC blends: reinforcement was only observed when an amorphous polymer was blended into a crystalline matrix. In the case of blending a crystalline polymer into an amorphous matrix, no adhesion was observed at the interface and the mechanical performance decreased upon blending. It is somewhat puzzling that the supposedly miscible PLA/PCL blend behaves like the immiscible HDPE/PC blend. However, the mechanism of reinforcement may not be due to interfacial bonding. For example, blending can change the mechanical properties of polymers by influencing factors such as crystallization kinetics. Also, the size of inclusions relative to the mean distance between them can strongly influence blend mechanical properties, even at constant interfacial adhesion [15]. To address this apparent inconsistency, DSC, SEM, and NMR experiments were performed in order to gain insight into the blend microstructure.

3.2. Thermal properties

The thermal properties of the blend were probed using DSC. In Fig. 6 scans for pure PLA, pure PCL, and a blend having mass fraction PLA of 0.2 are shown. The DSC traces from blended samples gave somewhat varied results, which might be attributed to the sensitivity of glass-forming liquids to the method of preparation [16]. The melting temperature of PCL is estimated to be 62°C and the glass transition temperature of PLA is 53°C, both consistent with literature values [1]. It was difficult to determine exactly the transition temperatures of the blends when the peaks overlap and in some samples peak broadening was observed, but two trends were apparent from these measurements: the T_g of PLA is essentially unchanged from that of the pure material and the T_m of PCL is unchanged or slightly lower. However, variability in the DSC traces, particularly around the PLA glass transition, suggests the blend has complicated phase behavior. The glass transition is a kinetic phenomenon that is strongly influenced by the local material environment [17] so based on these results we are unable to conclusively state whether this material is indeed phase-separated.

3.3. Electron microscopy of blend microstructure

Scanning electron microscopy was used to investigate directly the microstructure of the PLA/PCL blends. In Fig. 7(a), a micrograph of the sample with PLA mass

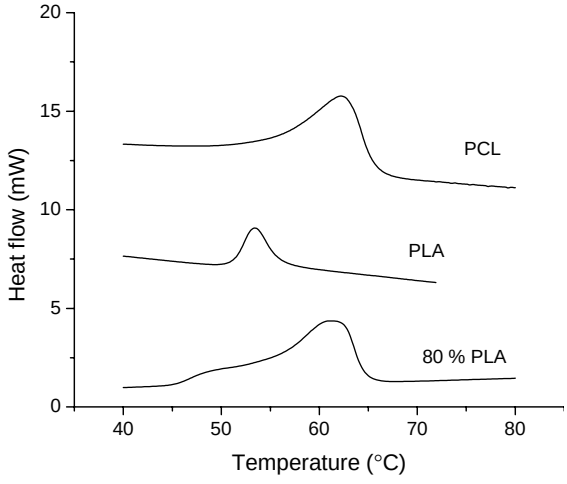

Fig. 6. Representative DSC traces for three samples, 100 PLA, 0 PLA and 20:80 PLA:PCL. Samples were heated at 10°/min under helium. The T_g of PLA is estimated to be 53°C and the T_m of PCL is 63°C. The T_m of PCL is largely unchanged but a shift to lower temperature and some broadening in the T_g of PLA is observed, which suggests some mixing may have occurred. The estimated uncertainty in these measurements is ±1°C.

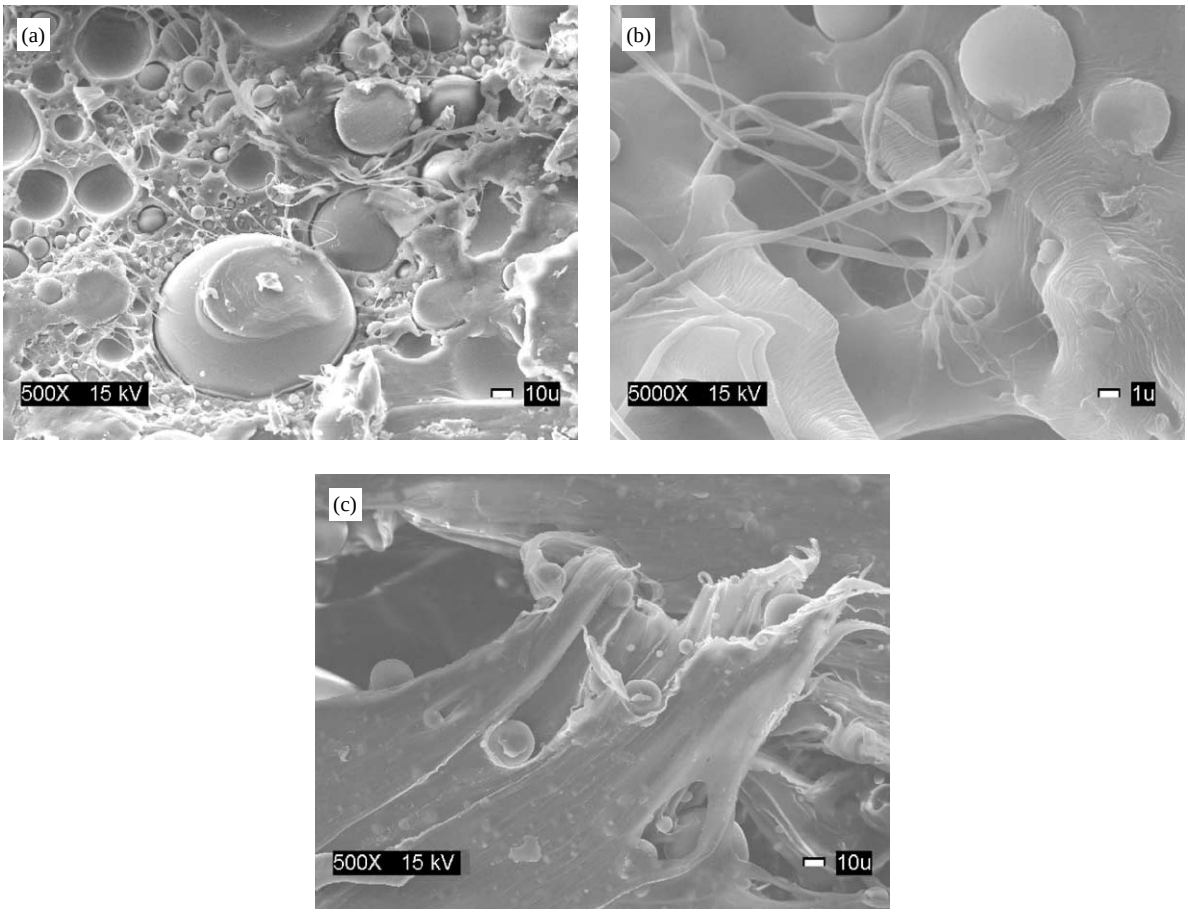

Fig. 7. (a) Scanning electron micrograph of the 40/60 blend at 500 × magnification. The blend is comprised of spherical inclusions in a continuous matrix. (b) Close-up image at 5000 × magnification of the blend. Striations visible in the matrix confirm it is primarily composed of PCL. The interface between the inclusions and the matrix is sharp, suggesting a lack of adhesion between blend components. (c) Image of the strained sample at 500 × magnification. No deformation in the spherical inclusions is observed, further suggesting little adhesion occurs between components.

fraction 0.4 is shown. The microstructure is characterized by relatively large, spherical inclusions of what is assumed to be PLA in a PCL matrix. The particles have diameters ranging from 5 μm to 100 μm and appear to be isolated from each other by the matrix.

In Fig. 7(b), a higher-magnification view of the same sample is shown. The crazing that is visible as well as the texture in the matrix phase is indicative of a crystalline polymer, consistent with the assertion that the matrix is rich in PCL as would be expected from the asymmetric blend composition. The interface between the spherical inclusions and the matrix appears to be clean, suggesting there is little adhesion between the two phases. This is consistent with the absence of strong shifts in the thermal transitions of the two polymers as determined by DSC.

In Fig. 7(c), a micrograph of the failure point for the 40/60 sample that was tested mechanically is shown. The failure occurred in the matrix and very little deformation is observed in the spherical PLA-rich phase, also suggesting the adhesion between the two phases is weak. The lack of adhesion is quite unexpected because these polymers have been shown to be miscible in the melt state [13]. While contraction due to the glass transition and crystallization of these polymers could certainly lead to weak interfaces, it would be surprising if it led to complete phase separation. To probe further the blend microstructure and assess the degree of mixing we used solid-state NMR.

3.4. NMR measures of blend mixing

The intimacy of mixing between PLA and PCL was monitored by both direct and indirect means. Mixing, if it occurs, is only expected between the PLA chains and the *non-crystalline* (NC) chains of PCL. Also, the fact that the mobility of the NC-PCL chains in pure PCL is, at ambient temperature, very much greater than that of the PLA chains, suggests that an intimate mixing of the two types of chains should result in some restriction of mobility for the NC-PCL segments and an increase in mobility for the PLA chains. Since linewidths in the Bloch-decay (broadline) spectra of solid polymers qualitatively relate to mobility, we will first examine

the component linewidths in the blend, relative to the homopolymers for evidence of such changes.

In Fig. 8, M_0 (corresponding to Boltzmann spin populations) Bloch-decay spectra of the pure PLA (8C), pure PCL (8B), and the spectrum of the 40/60 PLA/PCL blend (8A) are displayed. MAS frequency is 2.5 kHz. The scaling of spectra 8B and 8C, relative to 8A, is such that the total intensity of 8A equals the sum of the total intensities of 8B and 8C. Moreover, the ratio of total intensities for 8B and 8C corresponds to the theoretical proton ratio for a 40/60 (by mass) PLA/PCL blend. Thus, spectrum 8D (=8A−8B−8C) is the lineshape difference between the experimental spectrum and a spectrum (not shown) representing non-interacting component contributions. Note that the vertical scaling factors are given in the figure and that 8A and 8B are shown with two vertical amplifications. Also, the horizontally expanded central regions of spectra 8A and 8D are shown as insets.

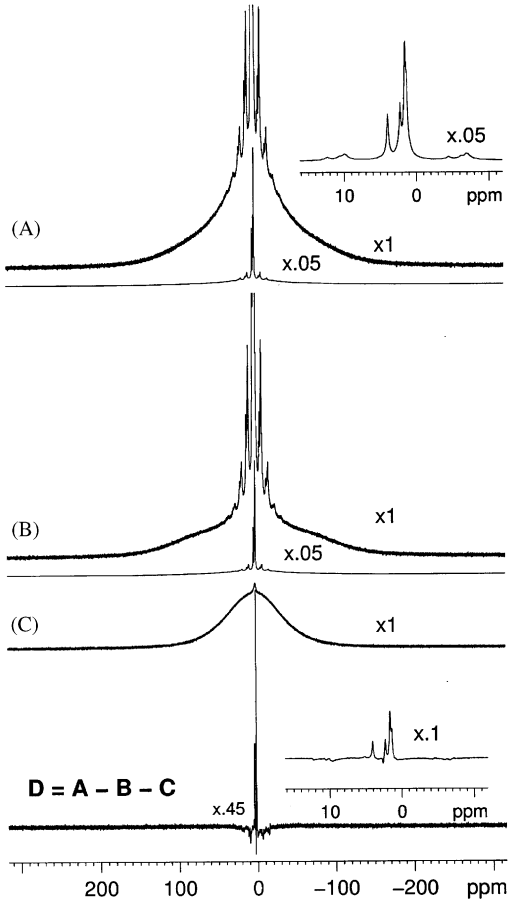

Fig. 8. 300 MHz Bloch-decay proton spectra of the 40/60 PLA/PCL blend (A), pure PCL (B) and pure PLA (C), with spectra B and C scaled to represent stoichiometrically weighted proton contributions to spectrum A. Thus, spectrum D represents the spectral difference between the blend spectrum and a spectrum consisting of non-interacting components. Vertical amplification factors are also shown. Insets in spectra A and D show the expanded central regions dominated by the highly mobile non-crystalline PCL protons. In spectrum A, the absence of narrowing associated with the PLA contributions and the absence of broadening for the non-crystalline PCL protons indicates a lack of intimate mixing.

The most relevant observations, relating to mixing of the PLA and PCL are the following: (a) The mobility contrast between crystalline and NC-PCL protons is striking. In 8B, the broad wings are associated with a rather rigid crystalline region while the highly resolved centerband, flanked by spinning sidebands that are spread in multiples of 2.5 kHz about the centerband (see inset 8A), indicates that the NC-PCL chains have weak dipolar couplings and near-isotropic mobility that is fast on the timescale of a few microseconds. This high mobility is seen in both the spectrum of PCL and of the blend. (b) The spectrum of PLA is narrower than that of crystalline PCL; nevertheless, the PLA spectrum represents a relatively rigid collection of chains, given that the PLA protons include 3 methyl and 1, rather isolated, methine proton. The fast rotation of the methyl protons about the methyl symmetry axis and the isolation of the methine proton reduces each of their dipolar linewidth contributions relative to, say, the linewidth contributions of the rigid methylene protons of crystalline PCL. (c) In spectrum 8D, the broad components from both crystalline PCL and from all of the PLA protons are accurately nulled; recognizable differences are restricted to the spectral region associated with the NC-PCL protons. From 8D, we can deduce that in the experimental blend spectrum (8A), the centerband is slightly narrower and more intense than in 8B while the spinning sidebands are slightly less intense than would be expected from summing the experimental PCL and PLA spectra. The most compelling deduction from Fig. 8, in our opinion, is that *intimate mixing between PLA and NC-PCL chains is negligible* for the following reasons: (a) there is no added motional averaging of PLA chains, (b) the PCL crystallinity level is not reduced by intimate mixing and (c) the linewidth of the NC-PCL chains is slightly narrower than for pure PCL whereas broadening would be expected from intimate mixing with stiffer PLA chains. (The narrowing is only slight and is certainly not a result of mixing.) Thus, the data of Fig. 8 indicate that phase separation exists. The question remains: on what spatial scale is the phase separation?

We also performed a so-called "chemical-shift-based" spin diffusion experiment [18,19], which is used to estimate domain size. However, given that the results could not, in the end, be used to estimate domain size for this blend, the experimental results, illustrated in Fig. 9, will be described very sketchily. We include these results only because they provide more information than the Bloch-decay spectra did on the degree of isolation between the PLA and the NC-PCL chains.

The proton spectra of Fig. 9 are combined rotation and multiple pulse spectroscopy [20] (CRAMPS)

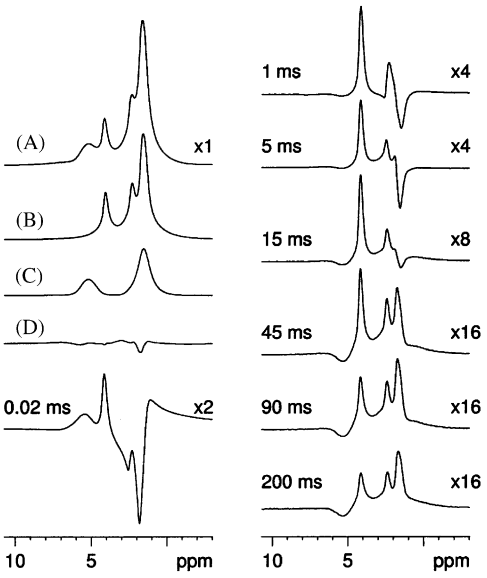

Fig. 9. CRAMPS spectra of the 40/60 PLA/PCL blend (A), the pure PCL (B), the pure PLA (C), all scaled to represent the weighted average of the components. (D) is the difference between the experimental spectrum and the stoichiometrically weighted sum of the component spectra. Remaining spectra are those associated with the chemical-shift-based spin diffusion experiment at the indicated spin diffusion times. Vertical amplification factors are included and are taken in reference to spectrum A. Of note is the constant amplitude of the negative, low-field PLA feature, indicating the total lack of spin diffusion between PLA and PCL protons. Also, the positive PCL contribution has a constantly changing lineshape indicating that dipolar interactions in the non-crystalline PCL regions are exceedingly small and unmodified by the presence of PLA.

spectra, which represents an approach to high-resolution proton NMR in solids. To a first approximation, the strong proton–proton dipolar couplings are eliminated by multiple pulse irradiation [21–23], in these spectra. Chemical shift effects survive and are reduced to isotropic shifts via MAS [24]. In Figs. 9A–C, the CRAMPS spectra of the 40/60 blend, pure PCL and pure PLA are, respectively shown. These spectra are scaled, as in Fig. 8, so that, the sum of 9B and 9C would equal 9A if the components did not interact. Spectrum 9D (=9A−9B−9C) is the difference spectrum showing that the blend spectrum, 9A, is close to being a simple sum of the component spectra. The remaining spectra of Fig. 9 are labeled by spin diffusion times, t_{sd}, and represent a selection of spectra obtained in the spin diffusion experiment.

Spin diffusion [25] can be observed when spectrally different protons have unequal average polarizations. Then, if the different types of protons are spatially proximate and connected via a network of proton–proton dipolar couplings, polarization will diffusively migrate from the region of higher polarization to that of lower average polarization. Based on the size and density of such dipolar couplings, spin diffusion constants can be associated with morphologically different regions of a sample. The extraction of domain size information from the experimental data then involves converting observed times required for spin equilibration into distances using diffusion equations and the known diffusion constants [26,27].

For the purposes of this paper, the important points about this one-dimensional "chemical-shift-based" spin diffusion experiment [19] are as follows: (a) an initial polarization profile is imposed on the system. This profile is basically the M_0 spectrum of the blend, multiplied by a sinusoidal function, whose phase and period are under experimental control. That initial profile is represented by the $t_{sd} = 0.02$ ms spectrum in Fig. 9. (b) Initially, polarization gradients exist between all chemically shifted protons, i.e. gradients exist both within the homopolymers and between the PLA and PCL protons. (c) Based on Fig. 8, we know that the PLA protons are relatively rigid; hence, we can expect [28] that after the first ms of spin diffusion, both methyl and methine PLA protons will have come very close to achieving internal spin equilibrium. Hence, for $t_{sd} \geqslant 1$ ms, we can monitor the average PLA polarization as a function of t_{sd} from intensity changes at the downfield edge (ca. 5–6 ppm) of the PLA methine–proton resonance. In Fig. 9, careful analysis shows that this negative, downfield PLA wing intensity does not change by spin diffusion towards the positive average PCL polarization. Rather, the only amplitude changes in the PLA polarization are small changes expected [26] from longitudinal proton relaxation. Thus, *in spite of a significant average polarization difference between PLA and PCL protons, no spin diffusion is seen over times of* 200 ms. (d) The spin equilibration among the highly mobile NC-PCL protons is exceedingly sluggish, taking well over 100 ms, as judged by the changing positive peak heights in the spin diffusion spectra. Hence, it is inappropriate to suggest that we know the spin diffusion constants in the NC-PCL domains. Without knowledge of the spin diffusion constant in one type of domain, it is also inappropriate in this case to estimate a lower limit on the domain size of phase separation. Spin diffusion constants have been investigated [29,30], for polymer phases with relatively high mobilities and it is found that these constants remain significant, even for very mobile systems. So a qualitative remark about PLA/PCL mixing is that *the results of* Fig. 9 *strongly suggest PLA/PCL phase separation on a scale significantly larger than the spacing between PCL crystallites.*

Finally, we also examined a 25/75 blend of PLA/PCL using the same battery of NMR experiments. Conclusions were identical to those for the 40/60 blend, suggesting proximity to the putative LCST phase boundary did not influence the results. Both the linewidth arguments and the lack of any observable spin diffusion point to phase separation on a scale larger

than the PCL long period. Thus we conclude that the interactions between PLA and PCL are minimal in these blends. The sensitivity of NMR is not sufficient to rule out small adhesive interactions at that interface between blend components but there is no evidence for PLA–PCL miscibility.

4. Conclusions

The mechanical properties of PLA–PCL blends can be tuned through the blend composition. The average modulus, strain-at-failure, and ultimate tensile strength may be continuously varied by almost an order of magnitude. Above a threshold PLA mass fraction of 0.4, the modulus and ultimate tensile strength increase almost linearly as a function of composition. This threshold may be due to strengthening of the blend interface in this regime but there was little evidence to support this in the SEM or NMR data. The strain-at-failure decreases monotonically with increasing PLA content, becoming flat above PLA mass fraction 0.6. The DSC and NMR results suggest that PCL still crystallizes at levels very similar to pure PCL. In addition, very little mixing occurs between PLA and the non-crystalline PCL. In fact, phase separation on a distance scale larger than the separation between PCL crystallites is indicated. We have used a percolation model to explain the observed mechanical properties. The percolation threshold appears to occur around a PLA mass fraction of 50%, above which PLA appears to form a continuous matrix. At low PLA mass fractions, the minority phase would be expelled from the PCL matrix forming isolated droplets. The DSC data for these samples tended to vary more but the SEM and NMR measurements on the 40% PLA samples found no evidence for mixing. These conflicting characterization results suggest that the phase behavior of PLA/PCL may be quite complicated. Our results suggest that PLA and PCL are not miscible and that some adhesion may occur at the PLA/PCL interface when the majority phase is PCL but not when it is PLA. Despite this, the range of mechanical properties accessed in these experiments demonstrates the utility of polymer blending.

Acknowledgements

The authors thank Dr. Carl Schulteisz, Dr. Donald Hunston, Dr. David McColskey, and Dr. Joannie Chin for helpful discussions and Mr. Anthony Guissipetti for assistance with performing the mechanical tests. MEB acknowledges the Summer Undergraduate Research Fellowship Program at NIST for support and NRW acknowledges the National Research Council Post-doctoral Fellowship Program at NIST for support.

References

[1] Engelberg I, Kohn J. Physico-mechanical properties of degradable polymers used in medical applications: a comparative study. Biomaterials 1991;12:292–304.
[2] Ward IM. Mechanical properties of solid polymers. New York: Wiley; 1983. 475p.
[3] Bucknall CB. Toughened plastics. London: Applied Science Publishers Ltd; 1977. 359p.
[4] Utracki LA. Polymer alloys, blends. Munich: Hanser Publishers; 1990. 356p.
[5] Paul DR, Barlow JW. Polymer Blends (or Alloys). J Macromol Sci Rev Macromol Chem 1980;C18:109–68.
[6] Willemse RC, Posthuma de Boer A, van Dam J, Gotsis AD. Co-continuous morphologies in polymer blends: the influence of the interfacial tension. Polymer 1999;40:827–34.
[7] Harris JE, Robeson LM. Miscible blends of poly(aryl ether ketone)s and polyetherimides. J Appl Polym Sci 1988;35:1877–91.
[8] Kunori T, Geil PH. Morphology–property relationships in polycarbonate-based blends. 1. Modulus. J Macromol Sci Phys 1980;B18:93–134.
[9] Kunori T, Geil PH. Morphology–property relationships in polycarbonate-based blends. 2. Tensile and impact strength. J Macromol Sci Phys 1980;B18:135–75.
[10] Leclair A, Favis BD. The role of interfacial contact in immiscible binary polymer blends and its influence on mechanical properties. Polymer 1996;37:4723–8.
[11] Kerner EH. The elastic and thermo-elastic properties of composite media. Proc Phys Soc 1956;69B:808–13.
[12] Uemura S, Takayanagi M. Application of the theory of elasticity and viscosity of two-phase systems to polymer blends. J Appl Polym Sci 1966;10:113–21.
[13] Meredith JC, Amis EJ. LCST phase separation in biodegradable polymer blends: poly(D,L-lactide) and poly(ε-caprolactone). Macromol Chem Phys 2000;201:733–9.
[14] Birley AW, Haworth B, Batchelor J. Physics of plastics: processing, properties, and materials. Munich: Hanser; 1991. 528p.
[15] Wu SH. Phase-structure and adhesion in polymer blends—a criterion for rubber toughening. Polymer 1985;26:1855–63.
[16] Angell CA. Formation of glasses from liquids and biopolymers. Science 1995;267:1924–35.
[17] Douglas JF. A dynamic measure of order in structural glasses. Comput Mater Sci 1995;4:292–308.
[18] Caravatti P, Neuenschwander P, Ernst RR. Characterization of heterogeneous polymer blends by 2-dimensional proton spin diffusion spectroscopy. Macromolecules 1985;18:119–22.
[19] Campbell GC, Vanderhart DL. Optimization of chemical-shift-based polarization gradients in H-1-NMR spin-diffusion experiments on polymer blends with chemically similar constituents. J Magn Reson 1992;96:69–93.
[20] Ryan LM, Taylor RE, Paff AJ, Gerstein BC. Experimental-study of resolution of proton chemical-shifts in solids-combined multiple pulse NMR and magic-angle spinning. J Chem Phys 1980;72:508–15.
[21] Waugh JS, Huber LM, Haeberlen U. Approach to high-resolution NMR in solids. Phys Rev Lett 1968;20:180–3.
[22] Mansfield P, Orchar MJ, Stalker DC, Richards KHB. Symmetrized multi-pulse nuclear magnetic resonance experiments in solids: measurement of the chemical shift shielding tensor in some compounds. Phys Rev B 1973;7:90–105.

[23] Rhim W-K, Elleman DD, Vaughan RW. Analysis of multiple pulse NMR in solids. J Chem Phys 1973;59:3740–9.
[24] Andrew ER, Bradbury A, Eades RG. Nuclear magnetic resonance spectra from a crystal rotated at high speed. Nature 1958;182: 1659.
[25] Abragam A. The principles of nuclear magnetism. London: Oxford University Press; 1961. 599p.
[26] VanderHart DL, McFadden GB. Some perspectives on the interpretation of proton NMR spin diffusion data in terms of polymer morphologies. Solid State Nucl Magn Reson 1996;7: 45–66.
[27] Schmidt-Rohr K, Spiess HW. Multidimensional solid-state NMR and polymers. London: Academic Press; 1994p.
[28] Vanderhart DL. Proton spin-diffusion studies of polymer blends having modest monomer size. 1. Polystyrene poly(xylylene ether), a miscible blend. Macromolecules 1994;27:2837–45.
[29] Spiegel S, Schmidtrohr K, Boeffel C, Spiess HW. H-1 spin-diffusion coefficients of highly mobile polymers. Polymer 1993;34:4566–9.
[30] Mellinger F, Wilhelm M, Spiess HW. Calibration of H-1 NMR spin diffusion coefficients for mobile polymers through transverse relaxation measurements. Macromolecules 1999;32:4686–91.